Applied Surface Science 484 (2019) 771–780

Contents lists available at ScienceDirect

Applied Surface Science

journal homepage: www.elsevier.com/locate/apsusc

Full length article

Unusual step meandering due to Ehrlich-Schwoebel barrier in GaN epitaxy on the N-polar surface

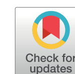

Henryk Turski[a,*], Filip Krzyżewski[b], Anna Feduniewicz-Żmuda[a], Pawel Wolny[a], Marcin Siekacz[a], Grzegorz Muziol[a], Caroline Cheze[c,1], Krzesimir Nowakowski-Szukudlarek[a], Huili (Grace) Xing[d], Debdeep Jena[d], Magdalena Załuska-Kotur[b], Czesław Skierbiszewski[a,c]

[a] *Institute of High Pressure Physics, Polish Academy of Sciences, Sokołowska 29/37, PL-01-142 Warsaw, Poland*
[b] *Institute of Physics Polish Academy of Sciences, Al. Lotników 32/46, 02-668 Warsaw, Poland*
[c] *TopGaN Ltd., Sokołowska 29/37, PL-01-142 Warsaw, Poland*
[d] *Cornell University, Ithaca, NY 14853, USA*

A R T I C L E I N F O

Keywords:
Step meandering
Ehrlich-Schwoebel barrier
Nitrides
Crystal morphology
Molecular beam epitaxy
Crystal growth modeling

A B S T R A C T

The stability of the Nitrogen-polar (000-1) surface of single-crystal bulk GaN substrates is studied for layers grown by plasma-assisted molecular beam epitaxy (PAMBE) in Nitrogen-rich conditions at 730 °C. It is shown that smooth GaN layers with parallel atomic steps are obtained for substrates when the surface crystal miscut angle is larger than 2°, revealing a highly stable epitaxial growth regime on single crystals. A step meandering pattern is observed on layers grown on lower miscut angle substrates. The meandering periodicity is found to have an inverse dependence on growth rate and miscut angle. This is *opposite* to what is observed for epitaxy on the Ga-polar surface. Combining analytic modeling and kinetic Monte Carlo simulations, it is shown that the existence of an Ehrlich-Schwoebel Barrier (ESB) in the PAMBE growth of GaN in nitrogen-rich conditions on (000-1) GaN reproduces the experimentally observed periodicity of step meandering. Assuming that ESB height depends on interactions between diffusing adatoms, all experimental phenomena are reproduced.

1. Introduction

Gallium Nitride (GaN) and the related family of semiconductors are attractive to scientists due to the wide range of applications in optoelectronic and electronic structures. Because GaN grows spontaneously in the wurtzite crystal structure, built-in large electronic polarization fields cause unique phenomena to appear in heterostructures that can be exploited for device design. Most commercially available devices such as transistors, light-emitting diodes and lasers have been developed on heterostructures grown along the Ga-polar orientation of the crystal with a few exceptions on non-polar and semi-polar structures [1,2]. Increasing interest is now directed to the N-polar orientation of the crystal, which can offer significant new possibilities over its Ga-polar counterparts, especially for electron blocking layer construction in light emitting devices [3,4] and the channel for two dimensional electron gas in high electron mobility transistors [5]. Recently, the growth of N-polar structures by metal-organic vapour phase epitaxy (MOVPE) has been reported, and a reduction in the background doping present in N-polar growth has been identified by introducing high miscut angle sapphire substrates [6–8]. Our work focuses on the growth of N-polar GaN layers on bulk GaN substrates by plasma-assisted molecular beam epitaxy (PAMBE). We show that growth on the N-polar surface opens new possibilities for obtaining high quality single crystal material by PAMBE depending critically on the miscut angle of the substrate. We observe a rich range of phenomena in the epitaxial growth dynamics for smaller miscut angle substrates, and explain these observations using analytical and kinetic Monte Carlo models.

Due to high diffusion barriers for nitrogen adatoms on the bare surface of GaN [9], metal-rich conditions are usually employed to obtain smooth GaN surfaces in PAMBE. As explained theoretically in [10], the presence of a metal adlayer at the surface of the GaN crystal significantly reduces the diffusion barriers for both Nitrogen and Gallium adatoms. Even though this “metal-rich” growth condition is widely used to successfully obtain device quality materials, it comes with a price. Careful monitoring of the presence of the metallic adlayer is necessary during epitaxial growth to prevent the formation of droplets occurring if the metal excess is too high. If the metal flux is too low, the wetting layer is partially lost, resulting in a rough surface. A different approach

* Corresponding author.
E-mail address: henryk@unipress.waw.pl (H. Turski).
[1] Now at Paul-Drude-Institut für Festkörperelektronik (PDI), Berlin, Germany.

https://doi.org/10.1016/j.apsusc.2019.04.082
Received 5 November 2018; Received in revised form 12 February 2019; Accepted 6 April 2019
Available online 09 April 2019
0169-4332/ © 2019 Elsevier B.V. All rights reserved.

to obtain smooth GaN layers was proposed in [11], where nominally slightly nitrogen-rich conditions were used in Ga-polar GaN growth at a high temperature. In this concept, the growth was carried out in the so called “wet surface N-rich” growth conditions, where the GaN surface decomposes significantly and metal layers are formed due to decomposition. In [12] it was pointed out, with a full growth diagram for Ga-polar GaN, that the dry surface in N-rich conditions results in rough surface, the so called 3D growth front of the crystal. On the other hand, in [13] it was presented that nucleation of first monolayer (ML) on Ga-polar GaN at low temperature is strongly affected by different conditions: N-rich, below 2 ML Gallium coverage and strongly Ga-rich - above 2 ML Ga coverage at the surface. For N-rich and less than 2ML Ga-adlayer conditions, a significant Ehrlich-Schwoebel barrier (ESB) was observed for diffusion over the single and double atomic steps, respectively. On the other hand no significant kinetic barrier was observed for > 2 ML Ga coverage of the surface. This observation shows an important role of the ESB [14] in the present work, where we investigate the growth kinetics of GaN under dry surface N-rich growth conditions in PAMBE.

Due to lower diffusion barriers expected for N-polar GaN compared to Ga-polar GaN [9], epitaxial layers were grown on N-polar (000-1) oriented bulk substrates at growth temperature of 730 °C. It is worth mentioning that for the Ga polar substrate orientation, in the temperature range 650-750 °C, successful growth of GaN is possible only for metal-rich conditions. In this temperature range GaN decomposition is negligible, so no Ga wetting layer can be formed out of the growing crystal. As shown theoretically in several works [15–17], kinetic barriers are also known to be the cause of periodic step meanders developing during the general process of crystal growth. Experiments carried out for GaN growth with excess Nitrogen on the Ga-polar surface by ammonia and plasma-assisted MBE as well as by MOVPE [18,19] show that, regardless of the growth technique, there exists a window of growth conditions in which meanders occur. Comparison between experimental observations and kinetic Monte Carlo (kMC) simulations indicate that the cause for meandering atomic steps is the ESB, which is significant during growth at relatively low temperatures. Moreover, for simple single component crystals, it is possible to determine the dominating ESB (atomic steps or kink) by analyzing the quantitative dependence of the topographic features such as the meander size (λ_m, presented schematically in Fig. 1) on the growth rate (V_{gr}), and the atomic terrace width (d), which is governed by substrate miscut angle (θ) [15,18]. In both cases, λ_m follows

$$\lambda_m \sim (d \bullet V_{gr})^{-\alpha} \approx \left(\frac{V_{gr}}{\theta}\right)^{-\alpha} \tag{1}$$

where $\alpha = 0.5$ for ESBs at atomic steps, and $\alpha = 0.25$ for ESBs at step kinks. The effect of the ESB for hexagonal GaN growth has been recently studied by kinetic Monte Carlo (kMC) simulations in [17]. For MBE growth under N-rich conditions on the Ga-polar surface, for conditions similar to MOVPE, a value of α close to 0.5 was obtained experimentally [19]. In the present study for N-rich GaN growth on N-polar (000-1) GaN surface we found, that the meander wavelength λ_m *increases* with increasing V_{gr}, and *decreases* with θ (implying a negative $\alpha = -0.5$ in Eq. (1)). Both these trends on N-polar growth are in disagreement with (i) theoretical predictions [15], (ii) kMC simulations [17,19] and (iii) results obtained by MBE and MOVPE growth of GaN on Ga-polar substrates [18,19]. We explain below an unusual behavior of λ_m with negative exponent α by presence of ESBs dependent on the interactions with other Ga adatoms located at the neighboring adsorption centers. It is well known from the study of the surface diffusion phenomena [13,20], that barrier height similarly as the depth of adsorption center can be changed by the presence of other adatoms, which as a consequence affects surface dynamics and determines the shape and stability of the surface. The combined experimental and modeling study reveals a growth phase diagram, including a growth window for the successful epitaxy of flat GaN layers by PAMBE in dry N-rich conditions on N-polar single crystals.

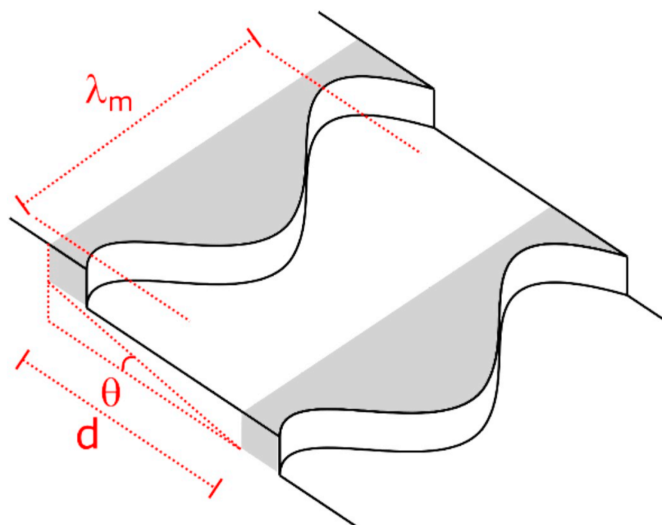

Fig. 1. Schematic image of the surface during growth. Miscut angle, step separation and meander periodicity are marked as θ, d and λ_m, respectively. The surface before growth is covered by parallel, equally spaced atomic steps. The gray shaded area denotes the grown part of the crystal.

2. Experimental

All samples in this study were grown by plasma-assisted MBE. To assure the same growth temperature, before each growth, the desorption time of the same amount of Gallium was confirmed by laser reflectometry [21]. The Ga desorption rates, as a function of the real substrate temperature was calibrated separately on 2-inch GaN/Al_2O_3 reference wafers using a k-Space Bandit pyrometer that measures temperature using the principle of blackbody radiation. Standard Ga sumo effusion cells are used to provide the molecular beam of Ga, while nitrogen is supplied by two radio frequency (RF) Veeco plasma sources. In the following, all fluxes are described in units of the equivalent growth rate (nm/min) for a sticking coefficient equal to 1. Growth rates were characterized in situ using oscillations of laser reflectometry signal for the same growth conditions on a separate GaN/Al_2O_3 Ga-polar template. The available nitrogen flux F_N, supplied by the two RF plasma sources, was between 6 nm/min (obtained for a single RF source) and 50 nm/min (for highest accessible N_2 flows and RF powers of both cells). Highest growth rate was achieved using 10 sccm N_2 flow and RF power of 500 W for both sources. To keep the pressure at a level compatible with MBE (10^{-5} Torr range), three CT10 cryopumps were used. The investigated samples were grown on bulk GaN substrates grown by the ammono-thermal method with threading dislocation density on the order of $10^4\ cm^{-2}$ to decrease the impact of substrate imperfections on the observed surface morphologies. N-polar surfaces were prepared for growth by mechanical and chemo-mechanical polishing to obtain atomic steps at miscut angles ranging from 0.5° to 4° towards the m-plane. For all growths, several bulk GaN pieces of at least 5 mm × 5 mm area were mounted with gallium or indium metal on a GaN/sapphire or silicon wafer, respectively. To allow for a fair comparison of obtained morphologies, 200 nm thick GaN layers were grown during each process. Surface morphology was studied using atomic force microscopy (AFM). Presented figures and measure of roughness as root mean square (RMS) values were obtained using software described in [22].

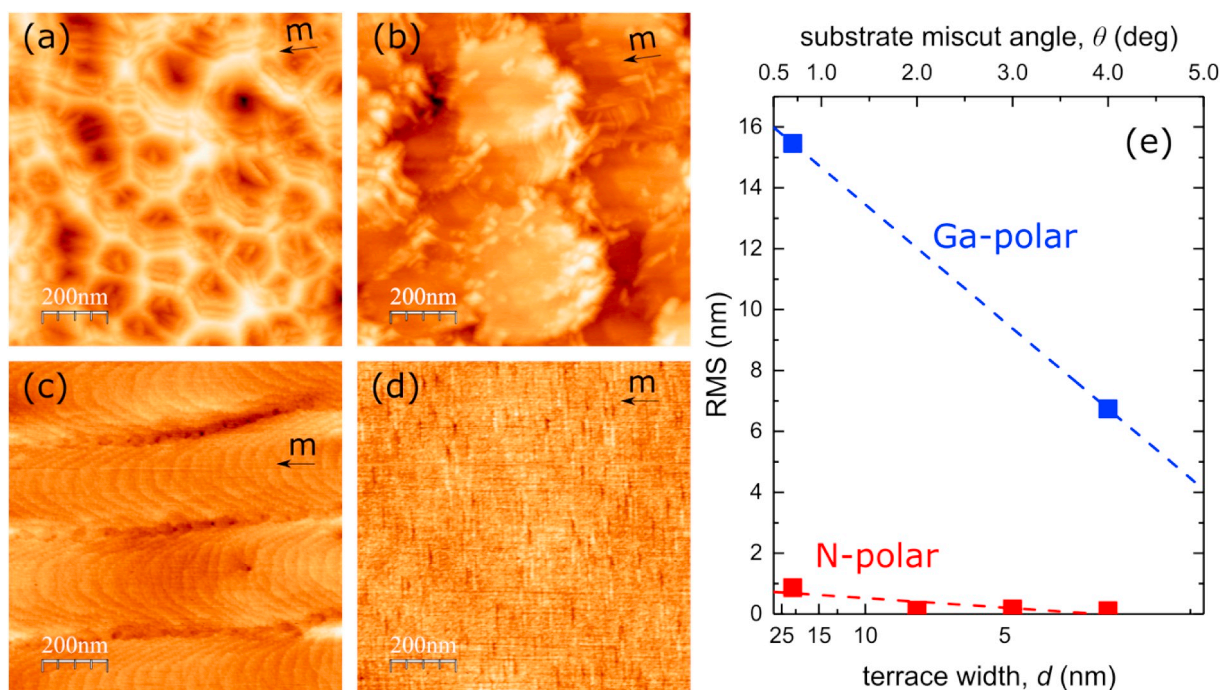

Fig. 2. GaN surface morphology obtained for substrate orientations: (a) Ga-polar $\theta = 0.7^{\circ}$, (b) Ga-polar $\theta = 4^{\circ}$, (c) N-polar $\theta = 0.7^{\circ}$, (d) N-polar $\theta = 4^{\circ}$. The samples were grown using fluxes: $F_{Ga} = 3.8$ nm/min, $F_N = 10$ nm/min. The color axis spans from 0 to (a) 40 nm, (b) 40 nm, (c) 5 nm, and (d) 2 nm. RMS values obtained for Ga- and N-polar growths are presented in (e). The Ga polar growths under N-rich conditions lead to rough surface morphologies, whereas for N-polar, smooth morphology with meanders are obtained for low substrate miscut angle, and smooth surfaces with no meanders are obtained for high substrate miscut angles.

3. Results

Typical meandered surface is schematically shown in Fig. 1. Miscut angle, meander length and terrace width are presented in this plot. The actual pattern that builds during surface dynamics depends on many parameters that characterize growth process. To highlight the significant difference between diffusion barriers for Ga- and N-polar surfaces, simultaneous growth of GaN was first carried out on Ga-polar (Fig. 2(a,b)) and N-polar (Fig. 2(c,d)) substrates with miscut angle θ equal to 0.7^{o} and $4^{o.}$ For the Ga-polar surface, growth resulted in a rough, three-dimensional structure without significant improvement for higher miscut angle. For the N-polar surface with miscut $\theta = 0.7^{o}$, a finger-like morphology was obtained with flat regions where atomic steps could be resolved (Fig. 2(c)). Similar structures have been reported previously [23]. Here in Fig. 2(d) we show that the morphology can be further leveled by using substrate with a higher miscut $\theta = 4^{o}$, which results in the disappearance of the finger like features and an RMS value of 0.11 nm, comparable to the substrate RMS before growth. RMS values obtained for Ga- and N-polar growth under N-rich conditions are presented in Fig. 2(e). This observation of smooth surface morphology obtained for GaN growth under N-rich conditions for high miscut angle substrates by PAMBE enables several new possibilities for applications of this technique. The growth can be carried out for many hours without the need for controlling the wetting layer (because there is none), which is quite distinct from the growth condition under Ga-rich conditions. This finding also brings N-rich growth conditions by PAMBE close to those for ammonia-MBE, where much higher nitrogen overpressures are used [18].

The most straightforward explanation of the result presented for N-polar substrates in Fig. 2(c) and (d) is that higher θ results in narrower atomic terraces, that shrink the path that Ga-adatoms need to travel to reach the atomic kink. Because of relatively low growth temperatures in PAMBE compared to ammonia-MBE and MOVPE, the Ga-adatom diffusivity on N-polar surfaces produces finger like morphology at small miscuts, which can be smoothed at higher θ with properly chosen fluxes of Galium and Nitrogen compounds, as will be shown later on.

Growth of N-polar GaN under N-rich conditions was then carried out at lower growth rates (lowering both F_{Ga} and F_N) to identify the growth window and find the lowest θ for which smooth growth without finger morphologies can be obtained. The results are presented in Fig. 3(a–c). The lowest θ for which the step-flow growth morphology was obtained is $\theta = 2^{\circ}$. As shown in Fig. 3(a-b), inter-step distance allows for distinguishing single atomic steps 0.25 nm high that dominate the surface. For Fig. 3(c), the extremely small terrace width due to the high miscut does not allow for reliable atomic step height measurement.

To understand the mechanism underlying the smoothing of N-polar GaN morphologies, growths were carried out on substrates with $\theta < 2^{\circ}$. Meandering atomic steps were obtained for a wide range of growth conditions. The AFM images in Fig. 4 show the resulting surface morphologies. A large change in the λ_m was obtained by varying atomic fluxes and the miscut θ. The meander periodicities obtained for the grown samples in this study have values similar to those observed by other authors for growth on the Ga-polar surface [19]. The morphologies of all layers grown in the step-meandering growth regime had similar RMS values of about 0.5–0.8 nm, and exhibited a regular, periodic sequence of meanders, with the exception of a sample grown at a very low growth rate ($F_{Ga} = 0.8$ nm/min) that resulted in a more irregular direction of meanders (Fig. 4(d)).

Step meanders are accompanied by valleys separating neighboring meanders. At the bottom of each valley, periodically arranged holes are visible. We believe that those holes are formed in the slowly growing part of the step meander by connecting adjacent meanders. The fact that holes are not filled during further growth but rather become deeper is a fingerprint of a high diffusion barrier blocking the downward diffusion over atomic steps.

The measured values of λ_m for all samples shown in Fig. 4 where step meandering was observed are presented in Fig. 5(a) as a function of the miscut, and in Fig. 5(b) as a function of the growth condition. As mentioned in the introduction, for all grown series of layers, λ_m follow

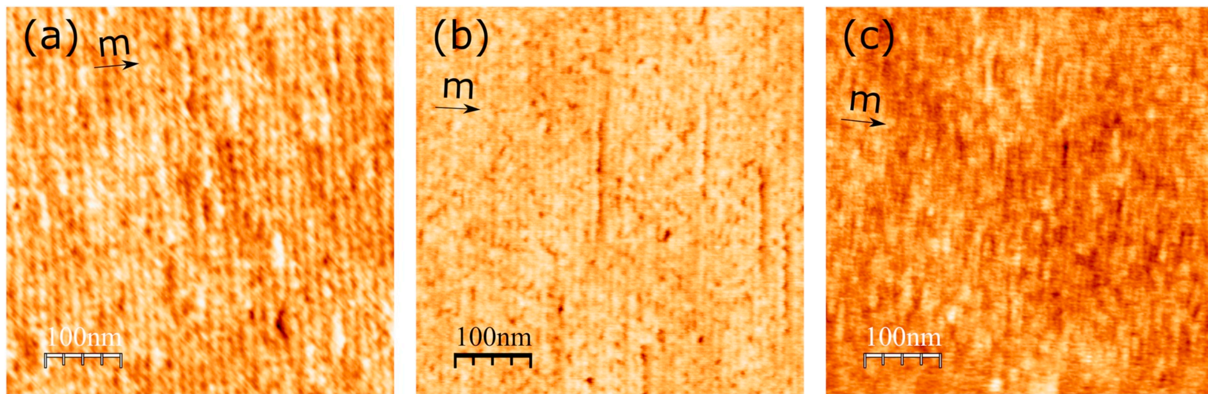

Fig. 3. Smooth surface morphologies obtained using F_{Ga} = 2.3 nm/min, F_N = 7.3 nm/min on N-polar substrates with (a) $\theta = 2^{\circ}$, (b) $\theta = 3^{\circ}$, and (c) $\theta = 4^{\circ}$. The vertical scale spans from 0 to: (a) 1 nm, (b) 2 nm, (c) 1 nm. Resulting RMS values are: (a) 0.12 nm, (b) 0.17 nm, (c) 0.11 nm. Smooth surface morphologies with no meanders are obtained for all three miscut angles.

Eq. (1) with negative value of exponent α. In fact, as shown in Fig. 5(b), close to a linear dependence of λ_m on $\sqrt{d \bullet \frac{F_{Ga}}{F_N}}$ was observed, which yields an unusual, inverse dependence of λ_m on θ and V_{gr} (defined here by F_{Ga}). The negative value of exponent α is in contrast to the positive values reported in past literature [15–19], whereas the proportionality to the square root of the appropriate combination of the growth parameters reflects the diffusional character of the dynamical processes at the surface. Value of F_N located in the denominator reflacts the reduction of Ga adatom diffusivity in the presence of higher Nitrogen excess on the surface. Depending on the assumptions made in the derivation of the formula expressing λ_m the combination of parameters that finally are under the square root is different [15,17,24,25]. We found that a simple relation of d, F_{Ga} *and* F_N fits very well to the data in the studied parameter range. In general, shorter terraces should lead to smoother growth and smaller step meandering. A crucial implication of our observation is that, at our growth conditions, narrower atomic terraces reduce the diffusivity of adatoms and lead to step meandering with shorter wavelength. Additionally we find that for extremely narrow terraces steps become straight. To understand this qualitative transition in growth regime that results in the smooth surface for high miscut angle substrates, we first use a simple analytical approach. Second, to describe the mechanism underlying the observed $\lambda_m(d, F_{Ga}, F_N)$ dependences, kMC simulations are employed. Using a relatively simple kMC model described below, we are able to reproduce qualitatively the changes of λ_m as a function of d, F_{Ga} and F_N. Note that

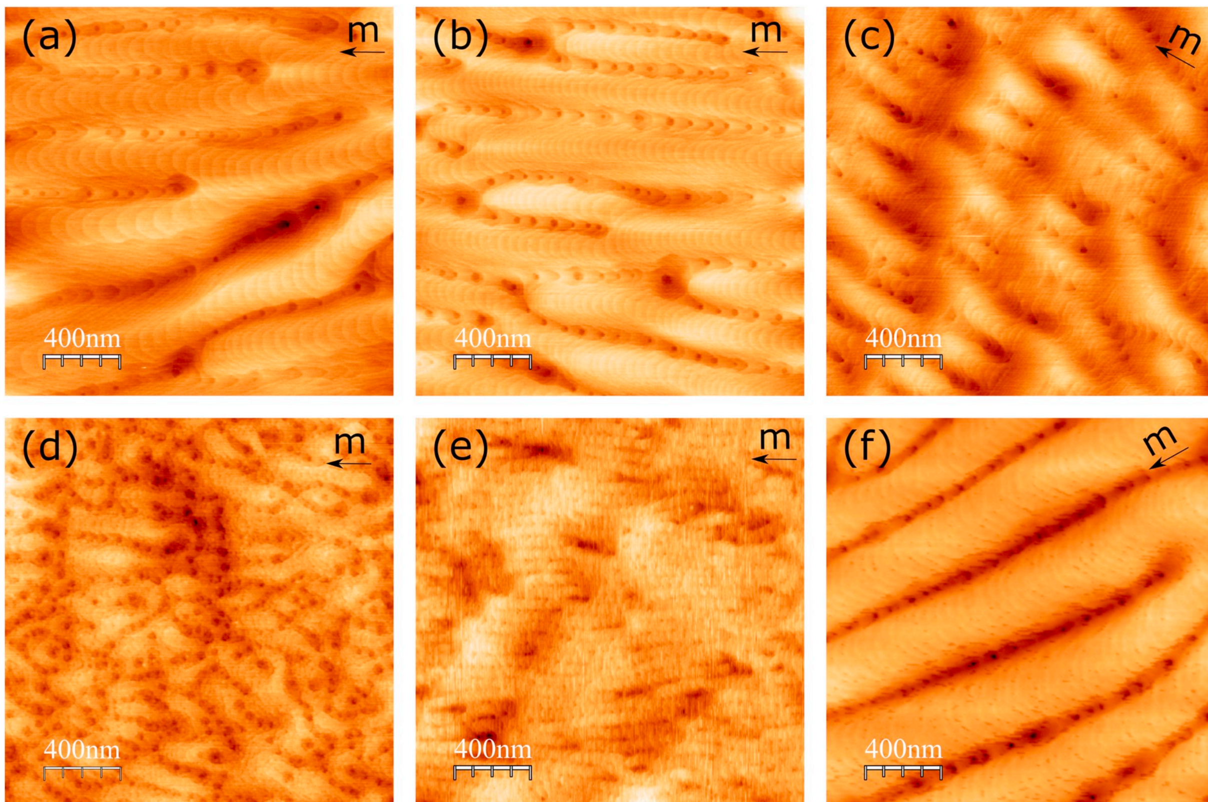

Fig. 4. Characteristic surface morphologies with varying meander periods obtained for N-polar grown GaN layers presented using the same lateral scale for low miscut angle substrates. Surface morphology shown is for F_{Ga} = 4 nm/min, F_N = 15 nm/min on substrates with (a) $\theta = 0.5^{\circ}$, (b) $\theta = 0.8^{\circ}$, (c) $\theta = 1.5^{\circ}$, (d) F_{Ga} = 0.8 nm/min, F_N = 15 nm/min, $\theta = 0.8^{\circ}$, (e) F_{Ga} = 4 nm/min, F_N = 50 nm/min, $\theta = 1.5^{\circ}$, (f) F_{Ga} = 3.2 nm/min, F_N = 7.3 nm/min $\theta = 0.7^{\circ}$. Images have different vertical range from 5 nm to 10 nm and the same lateral scale to easily present the features size.

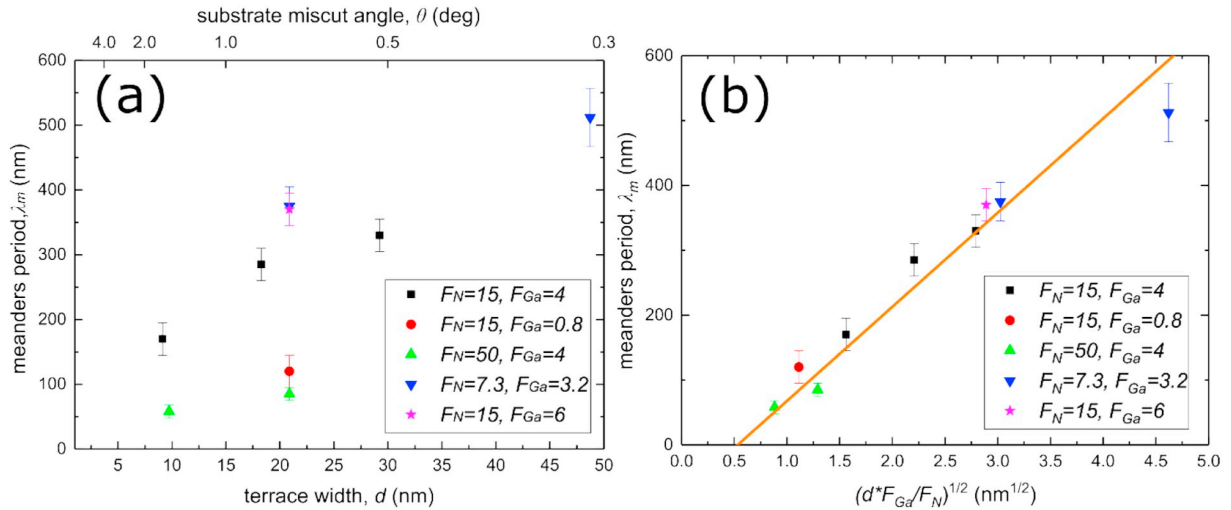

Fig. 5. Meander period as a function of (a) the terrace width d (or substrate miscut angle θ), and (b) the square root of the terrace width d multiplied by F_{Ga}/F_N (crystal growth rate equals F_{Ga}). The atomic fluxes used for the growths are indicated in the legend in units of nm/min. A linear fit to the experimental data is shown in (b) as a guide for the eye.

surface of miscut θ higher than 2° become smooth for low fluxes, even if according to the dependence in Fig. 5b they should create meanders with nonzero wavelength. We suppose that this is due to the decrease in amplitude of meanders for low fluxes and high miscut angle substrates. Such conditions lead to the occurrence of the stability window in the phase diagram, which will be analyzed later on.

3.1. Supersaturation in the presence of an Ehrlich-Schwoebel barrier

To show why change in surface morphology for high miscut angle substrates is expected, a very simple analytical approach is first used, in which only Ga adatoms are considered. We assume that the attachment of Ga adatoms is followed by a much faster attachment of N adatoms, making the process similar to monoatomic crystal growth described in the classic work [26]. The surface is approximated to be one dimensional with the x axis perpendicular to the atomic step edges, with atomic steps treated as uniform adatom sinks (growth centers) periodically separated (with period d) along the x axis. Then, as indicated in [26], the supersaturation at the surface ($\sigma_S(x)$) can be derived from the set of analytical equations:

$$x_s^2 \frac{d^2}{dx^2}\left(\frac{\sigma_S(x)}{\sigma}\right) = \frac{\sigma_S(x)}{\sigma} - 1 \tag{2}$$

$$x_s = a_0 \bullet \exp\left\{(W_S - U_S)/2k_B T\right\}. \tag{3}$$

Where σ is the supersaturation in vapour, x_s is a mean displacement of the adsorbed adatoms, W_S is the evaporation energy from the surface to vapour assumed to be equal to 2.2 eV [27], U_S is the diffusion barrier between the neighouring sites taken after [9] to be 1 eV for N-rich growth in the N-polar direction, and a_0 is the in-place lattice constant (0.3189 nm, [28]). From Eq. (3), the mean displacement of an adsorbed Ga adatom was calculated to be around $x_s \sim 330\,nm$ assuming $T = 730\,°C$.

To solve Eqs. (2) and (3) we need the boundary conditions for $\sigma_S(x)$. We assume that the attachment of adatoms from a lower terrace occurs with no kinetic barrier so after [26] we can write $\sigma_S(0) = 0$. For the adatoms diffusing through the edge ($x \to d$) we assume that there is ESB causing some non-zero supersaturation which results in $\frac{\sigma_S(d)}{\sigma} = \sigma_{S0}$. This is shown schematically in Fig. 6. We would like to point out that the σ_{S0} in our model is constant; it does not depend on growth parameters (other than T held constant at 730 °C).

Using the simple assumptions presented above, $\frac{\sigma_S(x)}{\sigma}$ was investigated. The obtained values are presented in Fig. 7(a) and (b) for fixed $d = 10\ nm$ and $\sigma_{S0} = 2 \cdot 10^{-4}$, respectively. The results presented in Fig. 7(a) show three qualitatively different supersaturation patterns. For low and negligible σ_{S0}, adatoms incorporate from both upper and lower terraces. For higher supersaturation, e.g. $\sigma_{S0} = 6 \cdot 10^{-4}$, $\frac{d\sigma_S}{dx}$ is > 0, indicating that statistically, adatoms adsorbed at the top terrace do not get incorporated into the lower atomic step. This qualitative difference that occurs for high σ_{S0} can be associated with a high ESB.

For the fixed $\sigma_{S0} = 2 \cdot 10^{-4}$, a similar qualitative change in the $\frac{\sigma_S(x)}{\sigma}$ pattern can be observed with reducing terrace width d. As presented in Fig. 7(b), for the used parameters, for $d \le 6.6$ nm (or in other words $\theta \ge 2.2°$) the derivative $\frac{d\sigma_S}{dx}(x) \ge 0$ indicating that statistically adatoms do not diffuse over steps (Fig. 6(a)). On the other hand, the absolute value of $\left.\frac{d\sigma_S}{dx}\right|_{x=d}$ increases with increasing d, indicating that for wide terraces (and fixed σ_{S0}), diffusion over atomic step becomes more probable (Fig. 6(b)).

The arbitrary choice of σ_{S0} values presented in Fig. 7 was dictated by the change in behavior of $\frac{\sigma_S(x)}{\sigma}$ for similar terrace widths as those resulting in the experimentally observed transition from meandering to parallel atomic steps. For higher and lower σ_{S0} values, the derivative $\frac{d\sigma_S}{dx}(x)$ will change sign for higher and lower d, respectively.

The simplified analysis of the growth process presented above indicates the correlation present between adatom density, terrace width and Schwoebel barrier. This gives a hint to a possible mechanism underlying the qualitative transition in growth morphologies observed experimentally for extremely thin atomic terraces (from meandering to parallel step edges, without any sign of meandering). As presented above, in the presence of ESB, for thin enough terrace, adatoms are incorporated into the atomic edge only from lower ledge. In comparison to the growth on wider terraces, this would completely change the kinetics of growth and presumably lead to parallel atomic steps.

It is important to point out that the reasoning is based on the nontrivial assumption that σ_{S0} does not change significantly with d. In general, the value of σ_{S0} depends on both the EBS and the terrace width d. Below, we present the kinetic Monte Carlo (kMC) model, which explains the observed surface transformations as a function of miscut angle and Ga and N fluxes by assuming that ESB changes by the interaction of the jumping adatom with the other adsorbed particles. As a result ESB height depends on the local density of adatoms.

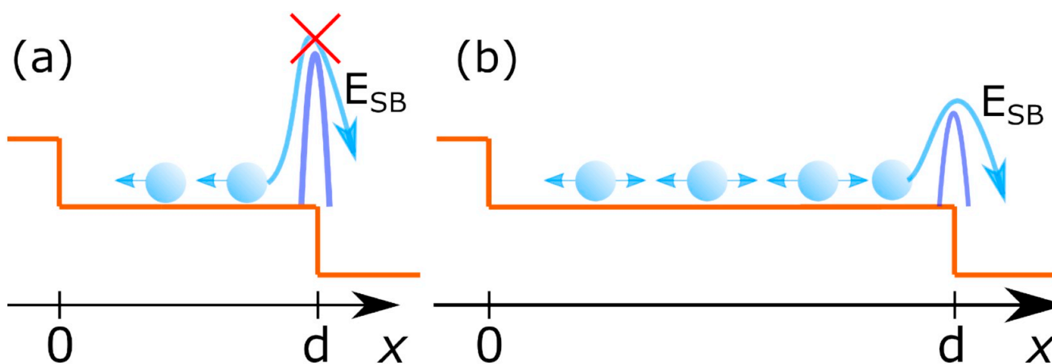

Fig. 6. Schematic picture showing the diffusion of adatoms in the presence of a Ehrlich-Schwoebel (E_{ESB}) barrier for (a) narrow and (b) wide atomic terrace. Statistically, for a narrow terrace (a), the Ehrlich-Schwoebel barrier causes all adatoms to incorporate into the upper step by effectively blocking diffusion over the atomic step.

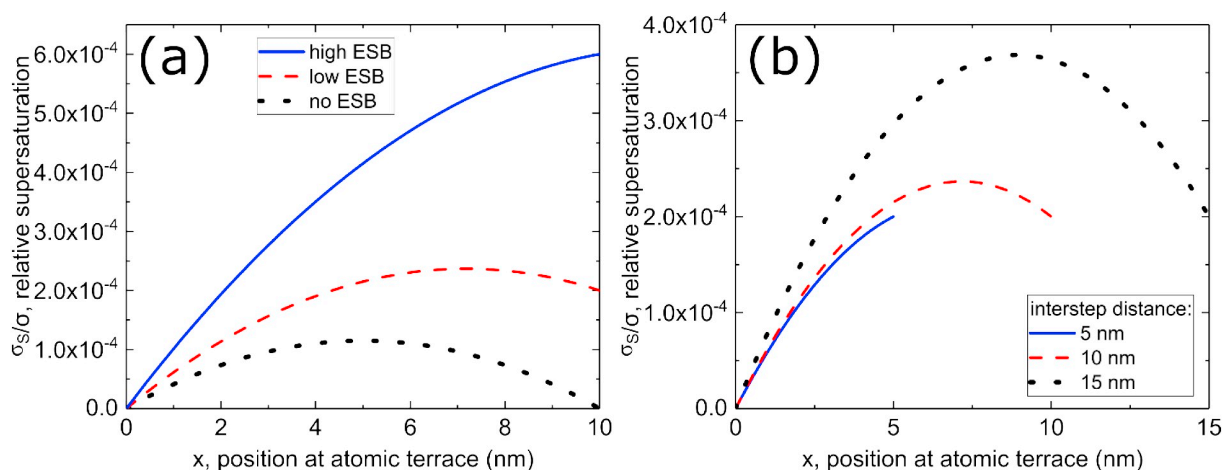

Fig. 7. (a) Relative supersaturation σ_S/σ vs position on an atomic terrace for a constant step separation ($d = 10\,nm$) and $\sigma_{S0} = 0$, $\sigma_{S0} = 2\cdot10^{-4}$ and $\sigma_{S0} = 6\cdot10^{-4}$ using dotted, dashed and solid plots, respectively. Atomic edges are located at $x = 0$ with no kinetic barrier (no inverted ESB), leading to $\sigma_S(0) = 0$ and at $x = 10\,nm$, where lower step edge with a varying ESB for over the step diffusion is presented. (b) Supersaturation vs position on an atomic terrace for various step separations and a constant $\sigma_{S0} = 2\cdot10^{-4}$. The upper atomic step is located at $x = 0$ with no kinetic barrier while the lower step is located at $x = 5\,nm$, $x = 10\,nm$ and $x = 15\,nm$ for solid, dashed and dotted plots, respectively.

3.2. Kinetic Monte Carlo simulations

To investigate the process of step meandering, we use a 2 + 1D kMC model presented in our previous manuscripts [29,30]. Each time step of the simulation consists of three stages. In the first stage, particles from external fluxes F_{Ga} and F_N are adsorbed at the surface. The second stage is that of diffusion. At the beginning of this step we calculate the jump probabilities of each particle (each lattice site). The probabilities P, are given by the formula:

$$P = \nu \bullet e^{-\beta\bullet(E+E_{ESB})} \quad (4)$$

where E is the total energy of bonds with nearest (NN) and next nearest neighbors (NNN) of the jumping particle [29,30]. NN bonds connecting Ga and N atoms are the strongest and $E_{GaN} = 1.6\,\text{eV}$. NNN bonds are significantly weaker; $E_{NN} = 0.3\,\text{eV}$ and $E_{GaGa} = 0.35\,\text{eV}$ for two nitrogen or two gallium atoms respectively. The system temperature T is contained in $\beta = 1/k_BT$ where k_B is the Boltzmann constant. E_{ESB} denotes the height of Ehrlich Schwoebel barrier, the additional barrier that is present close to the surface steps, thus it is equal to zero everywhere besides sites at the top of steps. Due to the inter-particle interactions its value in this model depends on the local particle surrounding, what will be discussed below. The parameter ν is time scaling prefactor which in the simulations has a value chosen in such a way that it allows to realize a fastest jump with probability $P = 1$. All data can be rescaled by multiplying by the appropriate scale factor. After the calculation of all jump rates, every move is executed with the appropriate probability. At the end of each time step, every lattice site is subjected to the process of sublimation. The desorption probabilities were set in a such a way that Ga atoms do not desorb at all (in agreement with the experimentally observed result that, within the tested temperature range, the growth rate does not change with growth temperature) and N atoms desorb relatively easy especially in the case when a single N atom does not have any Ga neighbor. The typical mechanism of Nitrogen desorption is when two Nitrogen adatoms stick together and desorb as a single molecule. We do not model the sticking process here, but in order to perform the resulting fast desorption process, we reduce the depth of the potential well where the atom resides, which is equal to the on-site particle bonding energy, about 2 eV. As a result, the desorption of N atoms is easier.

The Schwoebel effect [14] plays a crucial role in the model. It is well known [15–17] that in the presence of ESB, steps tend to meander. Our findings confirmed that $E_{ESB} = 0.5$ eV causes step meandering with wavelength growing with terrace width. Results are shown in Fig. 8. It can be seen that the effect is large: from 11° to 6°, the wavelength grows almost five times. Note that in this respect, the N-polar surface behaves differently than the previously studied Ga-polar one [17]. The source of the difference in this case can be assigned to the presence of large number of slowly diffusing N adatoms at the surface. Their presence actively slows down Ga particles in their movement across longer terraces, thus changing the length of created meanders. Next, we have

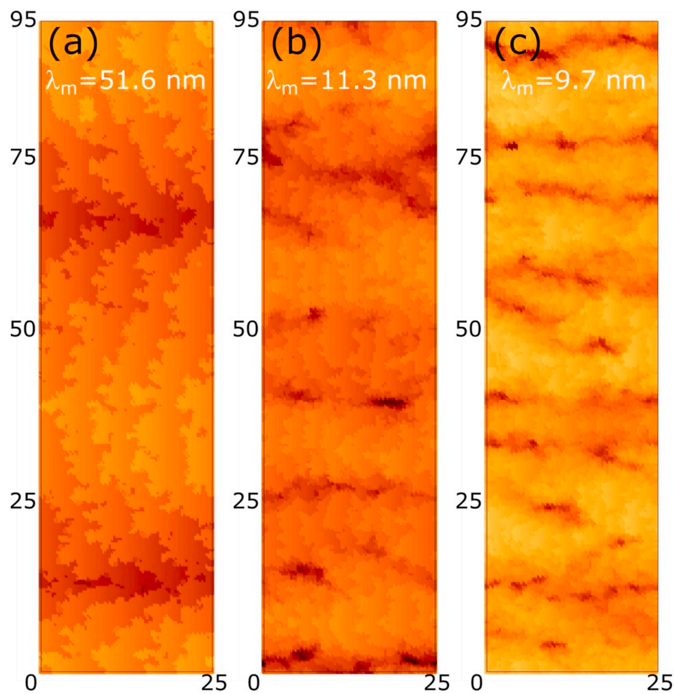

Fig. 8. Simulated morphology of N-polar GaN grown under N-rich conditions for substrate with: (a) 6°, (b) 11°, and (c) 18° miscut angle. Other growth parameters were kept constant: F_N = 16 nm/min, F_{Ga} = 0.1 nm/min, T_G = 750 °C. The simulation is performed using kinetic Monte Carlo, and is able to qualitatively reproduce the experimental morphology.

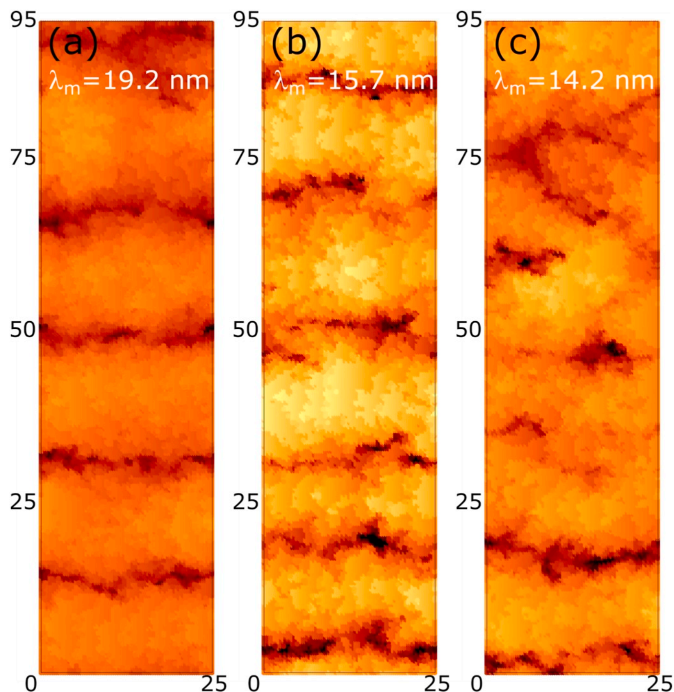

Fig. 9. Simulated morphology of N-polar GaN grown under N-rich conditions for F_N equal to (a) 16 nm/min, (b) 31 nm/min, and (c) 48 nm/min. Other growth parameters were kept constant: $\theta = 11^o$, F_{Ga} = 1.2 nm/min, T_G = 750 °C.

confirmed that an increase of Nitrogen flux causes a decrease in wavelength. The effect shown in Fig. 9 is not as spectacular as in the previous case, but careful analysis based on the correlation functions for three different samples in each case shows differences in the average meander length. Two of three experimentally found results - the miscut and nitrogen flux dependence - are reproduced within the model with one given value of ESB. In order to reproduce the experimentally found increase of wavelength as a function of Ga flux, we start by investigating the ESB height influence on the surface dynamics. Fig. 10 shows results for two different barriers E_{ESB} = 0.4 eV and E_{ESB} = 0.2 eV. It is clearly seen that height of ESB is important. Shape and size of meanders strongly depend on its value. In our model we assume that the ESB height is reduced by any Ga adatom that is close to the jumping particle. In such a way we reproduce expected properties of the studied surface. The argument behind this reasoning is that the neighboring adatoms usually interact with a jumping atom. They can change the whole energy landscape and as a result can affect also jump barriers. It is often found that the height of barrier for the jumping particle is changed due to the interactions with other particles that are present nearby [20]. In the same way, local energy potentials are modified by their presence. In our model we have assumed that Ga particles in the nearest neighborhood decrease ESB height. The ESB height reduction caused by large Ga coverage has been shown before on the Ga-polar (0001) GaN surface in the study of island nucleation process. It was found that diffusion over an atomic step strongly depends on the concentration of Ga adatoms [13]. In our model, each Gallium atom that moves across the step has to overcome the ESB which reduces the jump rate. If at least one Ga neighbor is present, the ESB becomes lower (0.1 eV); otherwise, the height of the barrier is 0.5 eV as shown in Fig. 11. It is important to point out that in a simplified picture presented in Fig 7, near the edge of the upper terrace in the presence of non-zero ESB (Fig. 7(a) near 10 nm), Ga adatom concentration can be also high and thus can lead to a significant reduction of the ESB. What means that in general case σ_{S0} would depend on both d and ESB.

Using the kMC model just described, we have investigated step meandering during the experimental N-rich growth conditions. The system temperature was kept constant at 750 °C, and the atomic fluxes and substrate miscut angle were varied in the simulation. The length of each simulation was chosen so that all layers had a thickness of 200 nm, consistent with the experiment. The simulated crystal morphologies are presented in Fig. 9, Fig. 10 and Fig. 12 in a series where θ, F_N and F_{Ga} are changed, respectively. The simple assumptions used to construct the model described above qualitatively reproduce the experimentally observed functional dependence of the meander on the parameters $\lambda_m(d, F_{Ga}, F_N)$ as shown in Fig. 13. The wavelength of meanders was read out from the height-height correlation plots calculated along the initial orientation of the steps. It has been shown before that such a method works very well for the studied surfaces [17]. Because size of systems studied by kMC model is much smaller than that observed experimentally, it was also necessary to reduce the magnitude of meanders in such a way that they could be created within the system. This is done by choice of rather high value of Schwoebel barrier. As shown below wavelength of meanders can be increased by decreasing of SB, thus allowing to approach the experimental values, if only large enough systems were studied. We can see however that even if λ_m studied by kMC model are much smaller than that experimentally measured, and they are obtained for much higher miscuts, the periodicity decreases with increasing F_N and θ while it increases with increasing F_{Ga}. As shown in Fig. 13, where λ_m is plotted as a function of rescaled parameters, all points besides one lie along the same line. In Fig. 14 growth for very low $F_{Ga}$and F_N for two different high miscuts are compared. It can be seen that at such conditions we approach stability window for very high miscut. We show that a little lower angle as in Fig. 14(b) already results in meandered steps. We believe that a quantitative agreement can be reached by adjusting the material parameters in the kMC model used here, though very little is currently known about the expected values for ESB or other energetic barriers governing the growth kinetics in the experimental process.

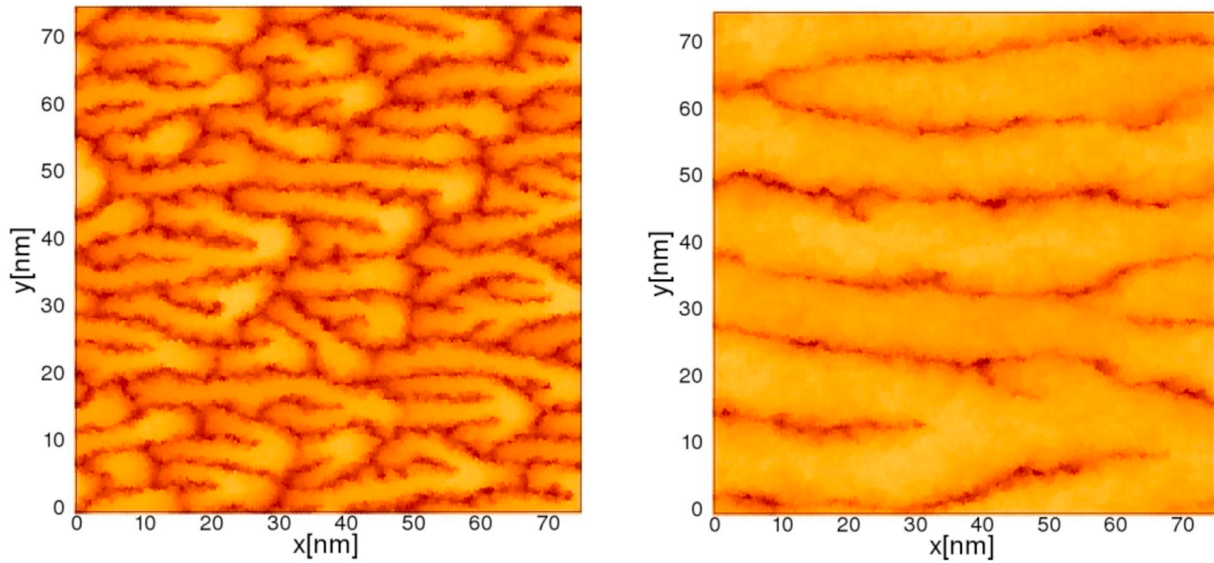

Fig. 10. Simulated morphology of N-polar GaN grown under N-rich conditions for, (a) E_{ESB} = 0.4 and (b) E_{ESB} = 0.2. Other growth parameters were kept constant: θ = 11°, F_N = 16 nm/min, F_{Ga} = 1.2 nm/min, T_G = 750 °C.

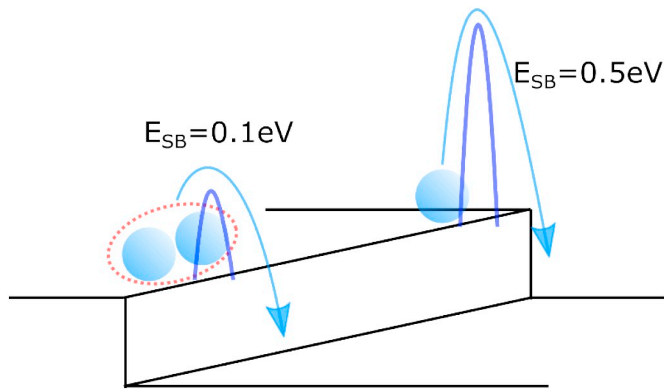

Fig. 11. Schematic picture showing the ESB = 0.5 eV near an atomic step for an isolated Ga adatom. When a neighboring site is occupied by another Ga adatom, the ESB reduces to 0.1 eV.

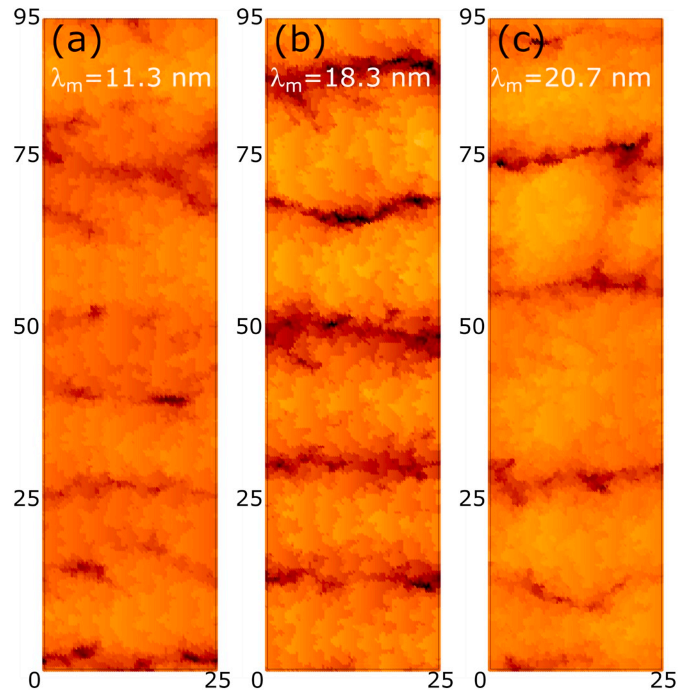

Fig. 12. Simulated morphology of N-polar GaN grown under N-rich conditions for F_{Ga} equal to (a) 0.1 nm/min, (b) 0.7 nm/min, and (c) 1.2 nm/min. Other growth parameters were kept constant: θ = 11°, F_N = 16 nm/min, T_G = 750 °C.

3.3. Growth diagram for N-polar GaN under N-rich growth conditions

To demonstrate how growth parameters define different morphologies obtained during N-rich growth on N-polar GaN substrates at a constant temperature, a growth diagram was constructed as shown in Fig. 15. The vertical scale depicts the relative excess of Nitrogen flux over Gallium flux $(F_N - F_{Ga})/F_N$, while the horizontal scale depicts the terrace width (and the miscut angle).

The growth diagram has much richer structure than could be concluded from the meander length analysis in Fig. 5. The morphologies in Fig. 15 are classified into four distinct categories: flat surface, meandering atomic steps, triangular/pyramidal islands and three-dimensional (3D). Examples of a flat surface were presented in Fig. 3.(a–c), meandering step edges in Fig. 2(c) and Fig. 4(a-f), and triangular islands are formed at conditions where meanders start to be flat (shown in Fig. 16(a,b)). 3D growth on the other hand was observed for low nitrogen flux excess over Ga flux and is shown in Fig. 16(c). The fact that 3D growth was obtained for $(F_N - F_{Ga})/F_N \approx 0.2$ provides evidence that indeed higher than that nitrogen excess is required for smooth growth morphology, while slightly N-rich growth results in rough surface commonly observed for N-rich Ga-polar growth by MBE.

Smooth surface morphology was obtained for a considerable number of samples grown on substrates with miscut angles between 4° and 2° for $(F_N - F_{Ga})/F_N \in (0.5, 0.75)$. Note that there are points in this parameter range that result in smooth surface, even if according to the plot presented in Fig. 5(b) they should meander with some, small wavelength. We speculate that the stability window is reached not only by coming with $\lambda_m \to 0$ but also by the decrease in the meander amplitude in the case of proper choice of $(F_N - F_{Ga})/F_N$. Decrease of meander amplitude with increasing miscut of the surface was analyzed in Ref. [17]. It was shown that amplitude is proportional to the square of

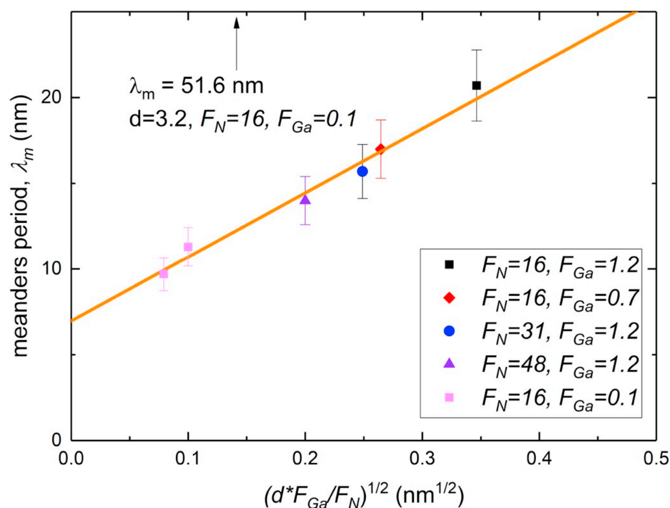

Fig. 13. Meander period of simulated systems plotted as a function of the square root of terrace width d multiplied by F_{Ga}/F_N (crystal growth rate equals F_{Ga}). A best-fit line is shown as a guide for the eye. Values of fluxes are given in nm/min units. For $d = 3.2$ nm, $F_N = 16$ nm/min and $F_{Ga} = 0.1$ nm/min, much higher meander period was obtained. This point has not been shown on the plot.

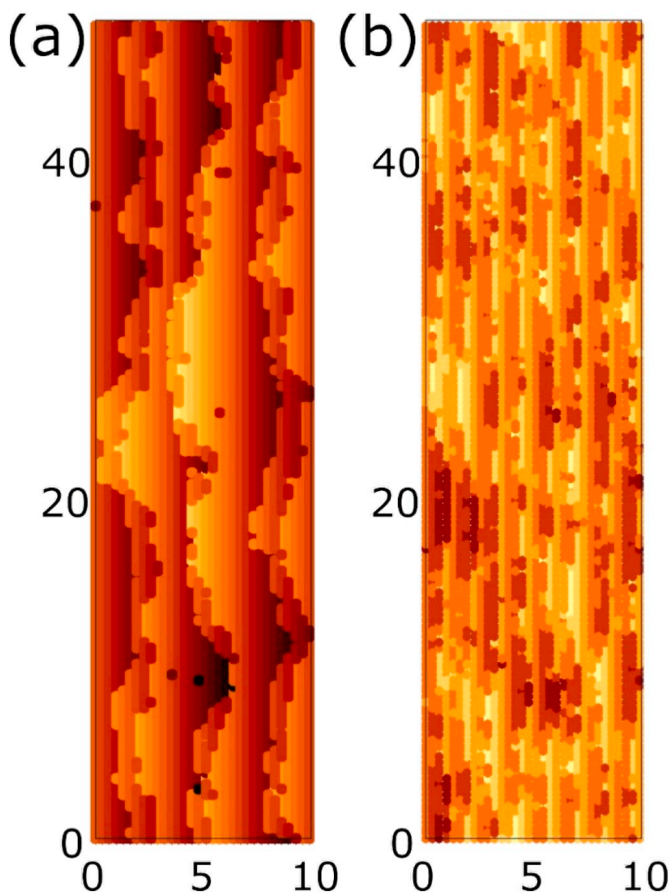

Fig. 14. Simulated morphology of N-polar GaN grown under N-rich conditions for substrate with: (a) $\theta = 10^{\circ}$ (b) $\theta = 40^{\circ}$. Other growth parameters were kept constant: $F_N = 0.32$ nm/min, $F_{Ga} = 0.01$ nm/min, $T_G = 750^{\circ}$.

terrace width and meander wavelength. In our case that would give the amplitude decrease as d^3. For higher $(F_N - F_{Ga})/F_N$ ratios, even for substrates with highest used miscut angle (4°), surface morphology

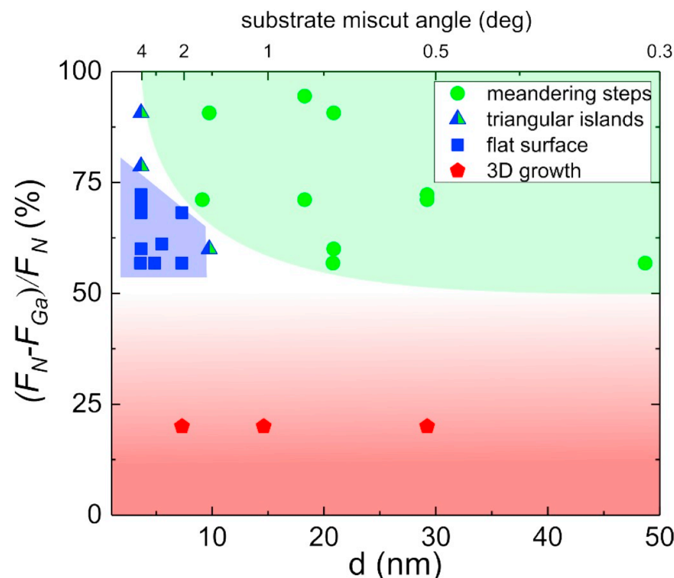

Fig. 15. Growth diagram summarizing various morphologies of GaN layers grown under Nitrogen conditions on single-crystal N-polar GaN substrates. The window of smooth and flat surface morphologies with no meanders lies in the window of miscut angles between 2 and 4°, and excess N fluxes from ~50–75%. This is an attractive N-polar growth window since it needs no stabilization and can be sustained for long growth runs while still reproducing a flat and atomically smooth surface.

became rougher due to the formation of triangular pyramids presented in Fig. 16(a).

4. Conclusions

In conclusion, the growth of GaN layers on N-polar substrates under Nitrogen-rich conditions by plasma assisted molecular beam epitaxy was studied. A growth window was identified for obtaining atomically flat surfaces at relatively low temperature (at which GaN does not decompose) for Nitrogen flux more than two times higher than Gallium flux. Since this N-rich growth condition does not require the stabilization of excess Gallium wetting layers, it can be sustained for long times and still result in atomically smooth surface morphologies without meanders and finger structures, essentially reproducing the surface structure of the underlying substrate. A lower diffusion barrier for N-rich growth on N-polar surfaces (compared to Ga-polar surfaces) was thus confirmed.

The key parameter enabling the transition between different observed morphologies was the miscut angle of the substrate. For relatively high miscut substrates ranging from 2° to 4°, smooth morphologies were obtained in a wide spectrum of other growth parameters. We propose that this transition is caused by ESB that, for short terrace widths, effectively blocks diffusion over steps. For step meandering obtained for GaN layers grown at lower miscut angles, an unusual meander width dependence on the growth rate and the substrate miscut angle was observed. Kinetic Monte Carlo simulations were carried out to assess the role of ESB on step meandering kinetics. We found that presence of excess Ga on the edges of atomic terraces can decrease the ESB for diffusion. Functional dependencies of λ_m on d, F_{Ga} and F_N were qualitatively reproduced by introducing an ESB that is dependent on the interactions with the other Ga adatoms, that are close enough. Existence of this ESB, which is responsible for inverted functional dependence of meander length on growth parameters, implies also the existence of unusual stability window for smooth N-rich growth on high miscut angle substrates.

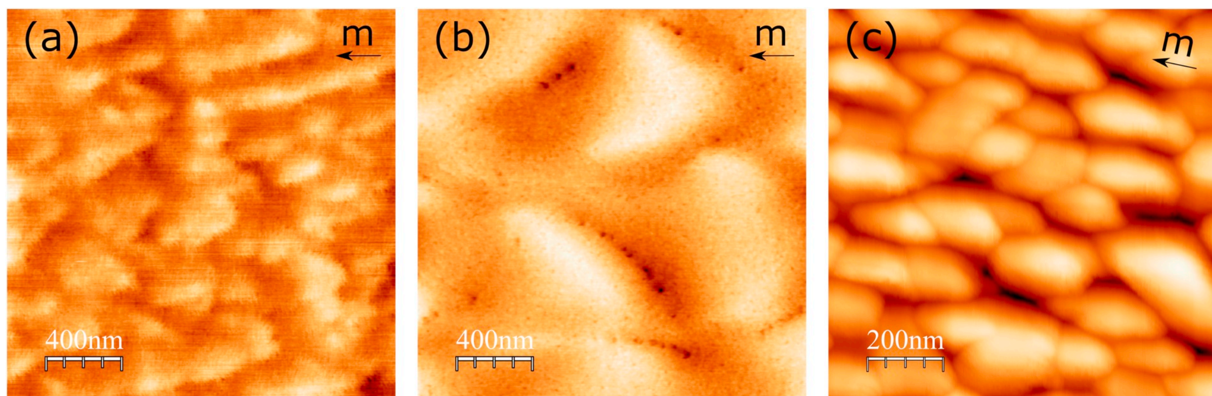

Fig. 16. Hillock morphology observed for N-rich, N-polar growth for different growth conditions: (a) F_{Ga} = 4 nm/min, F_N = 50 nm/min, $\theta = 4^{\circ}$, (b) F_{Ga} = 6 nm/min, F_N = 15 nm/min, $\theta = 1.5^{\circ}$, (c) F_{Ga} = 4 nm/min, F_N = 5 nm/min $\theta = 0.5^{\circ}$. The vertical axis spans from 0 to (a) 7 nm, (b) 9 nm and (c) 22 nm. RMS equals: (a) 0.8 nm, (b) 1.1 nm, and (c) 3.7 nm.

Acknowledgements

This work was supported by the Polish National Centre for Research and Development Grant PBS3/A3/23/2015, LIDER/29/0185/L-7/15/NCBR/2016, the National Science Centre (NCN) of Poland, Grant No. 2013/11/D/ST3/02700, the US AFOSR FA9550-17-1-0048, and the US NSF DMREF-1534303.

References

[1] K.M. Kelchner, S.P. DenBaars, J.S. Speck, GaN laser diodes on nonpolar and semi-polar planes, Advances in Semiconductor Lasers, 2012, pp. 149–182.
[2] M. Sawicka, G. Muziol, H. Turski, S. Grzanka, E. Grzanka, J. Smalc-Koziorowska, J.L. Weyher, C. Chèze, M. Albrecht, R. Kucharski, P. Perlin, C. Skierbiszewski, Ultraviolet laser diodes grown on semipolar (20$\bar{2}$1) GaN substrates by plasma-assisted molecular beam epitaxy, Appl. Phys. Lett. 102 (2013) 251101.
[3] J. Verma, J. Simon, V. Protasenko, T. Kosel, H. Grace Xing, D. Jena, N-polar III-nitride quantum well light-emitting diodes with polarization-induced doping, Appl. Phys. Lett. 99 (2011) 171104.
[4] D. Jena, J. Simon, A.K. Wang, Y. Cao, K. Goodman, J. Verma, S. Ganguly, G. Li, K. Karda, V. Protasenko, C. Lian, T. Kosel, P. Fay, H. Xing, Polarization-engineering in group III-nitride heterostructures: new opportunities for device design, Phys. Status Solidi A 208 (2011) 1511–1516.
[5] M.H. Wong, S. Keller, N.S. Dasgupta, D.J. Denninghoff, S. Kolluri, D.F. Brown, J. Lu, N.A. Fichtenbaum, E. Ahmadi, U. Singisetti, A. Chini, S. Rajan, S.P. DenBaars, J.S. Speck, U.K. Mishra, N-polar GaN epitaxy and high electron mobility transistors, Semicond. Sci. Technol. 28 (2013) 074009.
[6] C. Lund, S. Nakamura, S.P. DenBaars, U.K. Mishra, S. Keller, Growth of high purity N-polar (In,Ga)N films, J. Cryst. Growth 464 (2017) 127–131.
[7] C. Lund, B. Romanczyk, M. Catalano, Q. Wang, W. Li, D. DiGiovanni, M.J. Kim, P. Fay, S. Nakamura, S.P. DenBaars, U.K. Mishra, S. Keller, Metal-organic chemical vapor deposition of high quality, high indium composition N-polar InGaN layers for tunnel devices, J. Appl. Phys. 121 (2017) 185707.
[8] S.C. Cruz, S. Keller, T.E. Mates, U.K. Mishra, S.P. DenBaars, Crystallographic orientation dependence of dopant and impurity incorporation in GaN films grown by metalorganic chemical vapor deposition, J. Cryst. Growth 311 (2009) 3817–3823.
[9] J.N. Tosja Zywietz, Matthias Scheffler, Adatom diffusion at GaN (0001) and (000$\bar{1}$) surfaces, Appl. Phys. Lett. 73 (1998) 487–489.
[10] J. Neugebauer, T.K. Zywietz, M. Scheffler, J.E. Northrup, H. Chen, R.M. Feenstra, Adatom kinetics on and below the surface: the existence of a new diffusion channel, Phys. Rev. Lett. 90 (2003) 056101.
[11] G. Koblmüller, F. Wu, T. Mates, J.S. Speck, S. Fernández-Garrido, E. Calleja, High electron mobility GaN grown under N-rich conditions by plasma-assisted molecular beam epitaxy, Appl. Phys. Lett. 91 (2007) 221905.
[12] B.M. McSkimming, F. Wu, T. Huault, C. Chaix, J.S. Speck, Plasma assisted molecular beam epitaxy of GaN with growth rates > 2.6 μm/h, J. Cryst. Growth 386 (2014) 168–174.
[13] H. Zheng, M.H. Xie, H.S. Wu, Q.K. Xue, Kinetic energy barriers on the GaN(0001) surface: a nucleation study by scanning tunneling microscopy, Phys. Rev. B 77 (2008) 045303.
[14] R.L. Schwoebel, E.J. Shipsey, Step motion on crystal surfaces, J. Appl. Phys. 37 (1966) 3682–3686.
[15] C. Misbah, O. Pierre-Louis, Y. Saito, Crystal surfaces in and out of equilibrium: a modern view, Rev. Mod. Phys. 82 (2010) 981–1040.
[16] Y.-M. Yu, A. Voigt, X. Guo, Y. Liu, Simultaneous step meandering and bunching instabilities controlled by Ehrlich-Schwoebel barrier and elastic interaction, Appl. Phys. Lett. 99 (2011) 263106.
[17] M.A. Załuska–Kotur, F. Krzyżewski, S. Krukowski, Emergence of regular meandered step structure in simulated growth of GaN(0001) surface, J. Cryst. Growth 343 (2012) 138–144.
[18] N. Kaufmann, Investigation of Indium-rich InGaN Alloys and Kinetic Growth Regime of GaN, EPFL, 2013 PhD thesis.
[19] N.A.K. Kaufmann, L. Lahourcade, B. Hourahine, D. Martin, N. Grandjean, Critical impact of Ehrlich–Schwöbel barrier on GaN surface morphology during homoepitaxial growth, J. Cryst. Growth 433 (2016) 36–42.
[20] M.A. Załuska-Kotur, S. Krukowski, Z. Romanowski, Ł.A. Turski, Spreading of step-like density profiles in interacting lattice gas on a hexagonal lattice, Surf. Sci. 457 (2000) 357–364.
[21] M. Siekacz, A. Feduniewicz-Żmuda, G. Cywiński, M. Kryśko, I. Grzegory, S. Krukowski, K.E. Waldrip, W. Jantsch, Z.R. Wasilewski, S. Porowski, C. Skierbiszewski, Growth of InGaN and InGaN/InGaN quantum wells by plasma-assisted molecular beam epitaxy, J. Cryst. Growth 310 (2008) 3983–3986.
[22] I. Horcas, R. Fernandez, J.M. Gomez-Rodriguez, J. Colchero, J. Gomez-Herrero, A.M. Baro, WSXM: a software for scanning probe microscopy and a tool for nanotechnology, Rev. Sci. Instrum. 78 (2007) 013705.
[23] C. Chèze, M. Sawicka, M. Siekacz, H. Turski, G. Cywiński, J. Smalc-Koziorowska, J.L. Weyher, M. Kryśko, B. Łucznik, M. Boćkowski, C. Skierbiszewski, Step-flow growth mode instability of N-polar GaN under N-excess, Appl. Phys. Lett. 103 (2013) 071601.
[24] A. Pimpinelli, J. Villain, Physics of Crystal Growth, Cambridge university press Cambridge, 1998.
[25] D.H. Yeon, P.R. Cha, J.S. Lowengrub, A. Voigt, K. Thornton, Linear stability analysis for step meandering instabilities with elastic interactions and Ehrlich-Schwoebel barriers, Phys. Rev. E Stat. Nonlinear Soft Matter Phys. 76 (2007) 011601.
[26] W.K. Burton, N. Cabrera, F.C. Frank, The growth of crystals and the equilibrium structure of their surfaces, Philos. Trans. R. Soc. A Math. Phys. Eng. Sci. 243 (1951) 299–358.
[27] O. Ambacher, M.S. Brandt, R. Dimitrov, T. Metzger, M. Stutzmann, R.A. Fischer, A. Miehr, A. Bergmaier, G. Dollinger, Thermal stability and desorption of group III nitrides prepared by metal organic chemical vapor deposition, J. Vac. Sci. Technol. B 14 (1996) 3532–3542.
[28] I. Vurgaftman, J.R. Meyer, Band parameters for nitrogen-containing semiconductors, J. Appl. Phys. 94 (2003) 3675–3696.
[29] F. Krzyżewski, M.A. Załuska-Kotur, H. Turski, M. Sawicka, C. Skierbiszewski, Miscut dependent surface evolution in the process of N-polar GaN (000-1) growth under N-rich condition, J. Cryst. Growth 457 (2017) 38–45.
[30] F. Krzyżewski, M.A. Załuska-Kotur, Stability diagrams for the surface patterns of GaN(0001^{-}) as a function of Schwoebel barrier height, J. Cryst. Growth 457 (2017) 80–84.